ON THE FRACTURE MECHANICS OF PIEZOELECTRIC SOLIDS

HORACIO SOSA

Mechanical Engineering and Mechanics Department, Drexel University, Philadelphia,
PA 19104, U.S.A.

Abstract—A fracture mechanics analysis is developed within the realm of two-dimensional linear piezoelectricity. The asymptotic expressions for the electromechanical fields in the vicinity of the crack are deduced, and their behavior is illustrated through several examples. The modelling of the electric field's effects on crack arrest and crack skewing constitutes one of the important features of this article.

1. INTRODUCTION

In two previous articles in this Journal (Sosa and Pak, 1990; Sosa, 1991), the author considered some of the characteristics governing the electromechanical phenomena that arise in piezoelectric media containing defects. While the first article was concerned with a three-dimensional analysis of a transversely isotropic piezoelectric material with a crack, only the simplest configuration was studied: The crack front was assumed to be aligned with the material's axis of transverse isotropy (or poling axis). As a consequence, it was shown that only transverse shear stresses were affected by the electric field (and vice versa), despite the fact that the constitutive equations showed that these were not the only stress components interacting with the electric field. The search for a more general electromechanical coupling lead to the results presented in the second of the aforementioned references: An elliptical cavity was assumed to be embedded in the piezoelectric material with its generator parallel to an axis other than the poling axis. The assumption of plane strain conditions along the cylindrical generator resulted in the interaction of the in-plane mechanical and electrical variables. The perturbation of the stress and electric field components produced by the presence of elliptical and circular holes was studied in detail employing a complex variables approach. The present article can be regarded as a continuation of the author's work. Here the defect under study is a crack contained in a plane where full elasto-electric coupling takes place. Furthermore, the crack is viewed as the limiting case of an elliptical hole, and, therefore, the results previously obtained in terms of complex potentials can be extended in a straightforward manner. To render this paper self-contained a summary of these results is included in the Appendix.

The primary objective of this work is the development of an analytical model to describe the behavior of a crack contained in a piezoelectric material when subjected to electrical as well as mechanical loads. Towards this end, the stress and electric displacement distributions in the neighborhood of the crack are deduced. Moreover, fracture parameters of mechanical and electrical nature are introduced in a fashion commonly encountered in purely elastic fracture mechanics, which provide the dependence of the intensity of the elastic and electrical fields in terms of the crack geometry and loading conditions. As such, however, these parameters do not constitute a measure of the fracture resistance of the piezoelectric material. Numerical examples are provided to show electromechanical behavior in the vicinity of the crack under various loading conditions. In particular, it is shown that for certain ratios of electrical to mechanical load, the phenomena of crack arrest and of incipient crack skewing can be observed, thus confirming experimental observation.

It should be observed that despite the fact of its importance in areas such as the electronic and electromechanical industries, the literature on the fracture of piezoelectric materials addressed from an analytical point of view is still quite limited. Among the main contributions one can cite the works of Parton (1975), Deeg (1980), McMeeking (1989), Pak
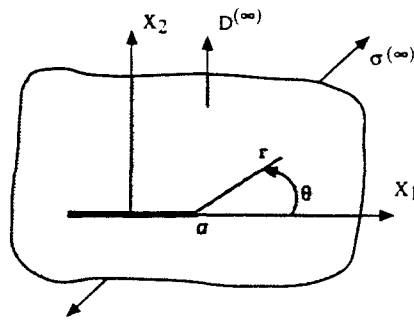
Fig. 1. Crack in a piezoelectric solid subjected to arbitrary electromechanical loads.

(1990, 1992), Shindo et al. 1990) and Suo et al. (1992). To the author's knowledge, however, this work is the only one that makes use of the complex potentials formulation.

2. CRACK IN A PIEZOELECTRIC SOLID

Consider an infinite piezoelectric medium of the class 6 mm (that is, transversely isotropic) referred to an x-, y-, z-rectangular coordinate system with constitutive equations given by

$$\varepsilon = s^D \cdot \sigma + g^T \cdot D,$$
$$E = -g \cdot \sigma + \beta^\sigma \cdot D \tag{1}$$

where ε, σ, D and E represent the strain, the stress, the electric displacement and the electric field, respectively. Moreover, s^D is the fourth rank compliance tensor measured at zero electric displacement, g is the third rank piezoelectric tensor, β^σ is the second rank dielectric impermeability tensor measured at zero stress and the superscript T denotes the transpose of a tensor. As previously observed by the author (Sosa, 1991), the assumption of plane strain conditions along the y-axis reduces (1) to a two-dimensional model whose constitutive equations in explicit form are given in the Appendix as (A1). In addition, and for notational purposes the x-z plane is relabelled x_1-x_2.

Consider a crack of length $2a$ embedded in this plane with its faces normal to the poling direction as depicted in Fig. 1. The piezoelectric solid is subjected to remote mechanical and electrical loads, and it is assumed that the faces of the crack are traction and surface charge free. Additionally, the crack can be thought of as being filled with a very thin layer of air, which has a dielectric constant approximately three times orders of magnitude smaller than the dielectric constants of the piezoelectric material. The consequence of such an assumption is that the boundary conditions on the faces of the crack are given by†

$$t = 0, \quad D \cdot n = 0, \quad \text{on} \quad x_2 = 0, \quad |x_1| \leqslant a, \tag{2}$$

where t is the stress vector and n is the unit outward normal to the crack faces.

As shown in the Appendix all the mechanical and electrical variables involved in the in-plane piezoelectric problem can be expressed in terms of three complex potentials $\varphi_j(z_j)$, $j = 1, 2, 3$, where $z_j = x_1 + \mu_j x_2$ is a generalized complex variable, and μ_j is a complex parameter which depends solely on the mechanical and electrical material properties of the piezoelectric solid. Recognizing the crack as the limiting case of the elliptical hole (A3) reduces to

---

†Discussions on the validity of the electrical boundary condition are given by Parton and Kudriatsev (1988) and McMeeking (1989).

$$\varphi_j(z_j) = (B_j + iB_j^*)z_j + \tfrac{1}{2}[-\Lambda_{j1}\sigma + \Lambda_{j2}\tau + \Lambda_{j3}\mathscr{D}]\{z_j - \sqrt{z_j^2 - a^2}\}, \tag{3}$$

where the following notation applies: $\sigma_{22}^{(x)} = \sigma$, $\sigma_{12}^{(x)} = \tau$ and $D_2^{(x)} = \mathscr{D}$. It should be noted that although (3) is valid for all values of z_j, it is the terms with explicit dependence on the applied load that will eventually dominate in the neighborhood of the crack tip. It follows then, that in this region loads such as $\sigma_{11}^{(x)}$ and $D_1^{(x)}$ will not be perturbed by the crack, as physical intuition suggests.

Using (3), (A8) and (A9) the components of σ and D can be obtained everywhere in the cracked piezoelectric solid. For example, algebraic manipulation shows that under general loading conditions $\sigma^{(x)}$ and $D^{(x)}$ the following expressions are obtained along the crack plane:

$$\sigma_{22}(x_1,0) = \begin{cases} 0 & \text{if } |x_1| < a, \\ \dfrac{\sigma x_1}{\sqrt{x_1^2 - a^2}} & \text{if } |x_1| > a, \end{cases} \tag{4}$$

and

$$D_2(x_1,0) = \begin{cases} 0 & \text{if } |x_1| < a, \\ \dfrac{\mathscr{D} x_1}{\sqrt{x_1^2 - a^2}} & \text{if } |x_1| > a. \end{cases} \tag{5}$$

Equation (4) expresses that along the crack line, the normal component of stress is independent of material properties as well as of the electrical load. Naturally, this will not be the case when $x_2 \neq 0$ because of material anisotropy and electromechanical coupling. In fact, it can be shown that the piezoelectric effect tends to increase the magnitude of the stress components. Likewise, (5) shows a similar independence of D_2 with respect to the applied stress.

As was mentioned in the Introduction, the main objective of this analysis is to study the distribution of the electromechanical fields in the vicinity of the crack tip. For this purpose, it is convenient to introduce polar coordinates r and θ with origin at the right crack tip as shown in Fig. 1. Using the relations

$$x_1 = a + r\cos\theta, \quad x_2 = r\sin\theta, \quad r > 0, \quad -\pi \leqslant \theta \leqslant \pi \tag{6}$$

and assuming that $r/a \ll 1$, the following approximations can be made:

$$z_j \simeq a, \quad \sqrt{z_j^2 - a^2} \simeq \sqrt{2ar}\sqrt{\cos\theta + \mu_j \sin\theta}. \tag{7}$$

Hence, the crack-tip expressions for the derivatives of the complex potentials become

$$\varphi_j'(z_j) = \frac{\sqrt{a}}{2\sqrt{2r}}[\Lambda_{j1}\sigma - \Lambda_{j2}\tau - \Lambda_{j3}\mathscr{D}] \frac{1}{\sqrt{\cos\theta + \mu_j \sin\theta}}. \tag{8}$$

Introducing the notation

$$C_j = \Lambda_{j1}K_1 - \Lambda_{j2}K_{11} - \Lambda_{j3}K_e, \tag{9}$$

where

$$K_1 = \sqrt{a}\sigma, \quad K_{11} = \sqrt{a}\tau, \quad K_e = \sqrt{a}\mathscr{D} \tag{10}$$

eqns (A8) and (8) yield the crack-tip stress distribution, namely

$$\sigma_{11} = \frac{1}{\sqrt{2r}} \Re \sum_{j=1}^{3} \frac{C_j \mu_j^2}{\sqrt{\cos\theta + \mu_j \sin\theta}},$$

$$\sigma_{22} = \frac{1}{\sqrt{2r}} \Re \sum_{j=1}^{3} \frac{C_j}{\sqrt{\cos\theta + \mu_j \sin\theta}},$$

$$\sigma_{12} = -\frac{1}{\sqrt{2r}} \Re \sum_{j=1}^{3} \frac{C_j \mu_j}{\sqrt{\cos\theta + \mu_j \sin\theta}}. \tag{11}$$

while (A9) with (8) give

$$D_1 = \frac{1}{\sqrt{2r}} \Re \sum_{j=1}^{3} \frac{C_j \mu_j \lambda_j}{\sqrt{\cos\theta + \mu_j \sin\theta}},$$

$$D_2 = -\frac{1}{\sqrt{2r}} \Re \sum_{j=1}^{3} \frac{C_j \lambda_j}{\sqrt{\cos\theta + \mu_j \sin\theta}} \tag{12}$$

with the coefficients λ_j being functions of the material properties as given by (A6). Clearly, similar expressions can be obtained for ε and E as well as for the elastic displacement u and the electric potential ϕ. These last two variables, however, are of order $r^{1/2}$ and, therefore, bounded. The important feature of eqns (11) and (12) is that they possess the elements present in the theory of anisotropic fracture mechanics: The characteristic singularity at the crack tip is of order $r^{-1/2}$, and the stress distribution near the crack tip depends not only on the geometry and loading, but on the material properties as well, as indicated by the coefficients C_j. The similarities with anisotropic fracture mechanics justify the definitions introduced in (10): K_I, K_{II} and K_e constitute fracture parameters which depend solely on the applied load and the geometry of the crack, and are referred to as the "mechanical intensity factors" for modes I and II and the "electrical intensity factor", respectively.

It should be noted that if one neglects piezoelectric and dielectric effects, the results given by (11) reduce to those of purely elastic anisotropic fracture mechanics, where only two complex potentials need to be considered [see for example Sih and Liebowitz (1968)].

3. EXAMPLES

Equations (11) and (12) reflect the qualitative behavior of σ and D in the vicinity of a crack. In this section, several examples are provided which quantify the effect of electric fields on crack propagation. Towards this end a piezoelectric ceramic known as PZT-4 is considered. The material constants are taken from Berlincourt et al. (1964) and in turn inserted into (A2). As is customary in fracture mechanics, the behavior of σ and D is better illustrated in terms of polar components. In such a case (11) and (12) reduce to

$$\sigma_{\theta\theta} = \frac{1}{\sqrt{2r}} \Re \sum_{j=1}^{3} C_j (\cos\theta + \mu_j \sin\theta)^{-1/2},$$

$$\sigma_{rr} = \frac{1}{\sqrt{2r}} \Re \sum_{j=1}^{3} C_j (\cos\theta + \mu_j \sin\theta)^{-1/2} (\sin\theta - \mu_j \cos\theta)^2,$$

$$\sigma_{r\theta} = \frac{1}{\sqrt{2r}} \Re \sum_{j=1}^{3} C_j (\cos\theta + \mu_j \sin\theta)^{-1/2} (\sin\theta - \mu_j \cos\theta), \tag{13}$$

and

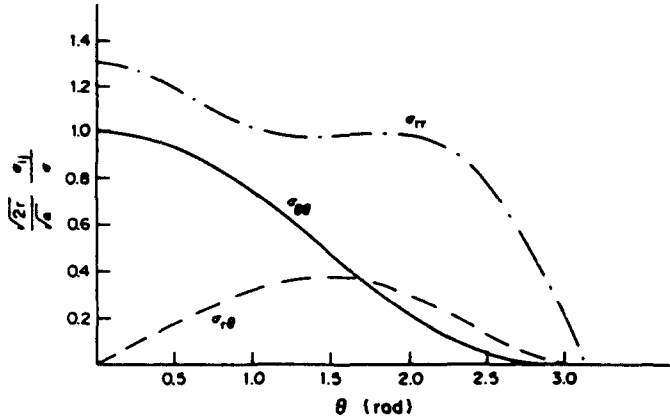Fig. 2. Stress behavior under a tensile load.

$$D_r = -\frac{1}{\sqrt{2r}} \mathfrak{R} \sum_{j=1}^{3} C_j \lambda_j (\cos\theta + \mu_j \sin\theta)^{-1/2}(\sin\theta - \mu_j \cos\theta),$$

$$D_{\theta} = -\frac{1}{\sqrt{2r}} \mathfrak{R} \sum_{j=1}^{3} C_j \lambda_j (\cos\theta + \mu_j \sin\theta)^{1/2}. \tag{14}$$

The following loading conditions are studied:

3.1. Far-field mechanical load

In this case let $\sigma_{22}^{(c)} = \sigma > 0$ be the only component of the applied stress. Therefore $C_j = \Lambda_{k1}K_1$. It is well known that a crack embedded in an isotropic material will tend to propagate in a self-similar manner along a path normal to the direction of maximum tensile stress, that is, along the plane $\theta = 0$. When the material is anisotropic that is not the case, and the material planes where the tensile load $\sigma_{\theta\theta}$ is a maximum must be determined. Figure 2 shows the normalized values of the stress components for $0 \leqslant \theta \leqslant \pi$. Notice that as predicted by (4) the maximum tensile stress occurs immediately ahead of the crack tip, and is independent of electrical effects. Figure 3 depicts the corresponding angular behavior of the electric displacement components induced by the application of the tensile load. Note that a value of $\sigma = 10^7 \mathrm{N}\ \mathrm{m}^{-2}$ will produce an electric displacement $\mathbf{D}$ of the order of $10^{-3}\ \mathrm{C}\ \mathrm{m}^{-2}$. The corresponding value of the induced electric field $\mathbf{E}$ can be found from (A10). The maximum value of D_{θ} occurs at approximately $\theta = 110°$ when $D_r = 0$.
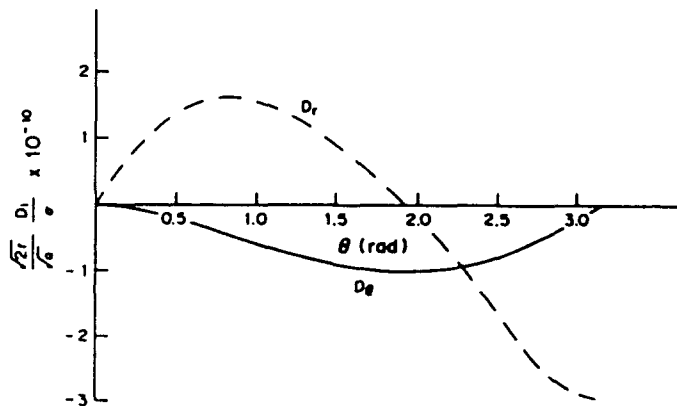

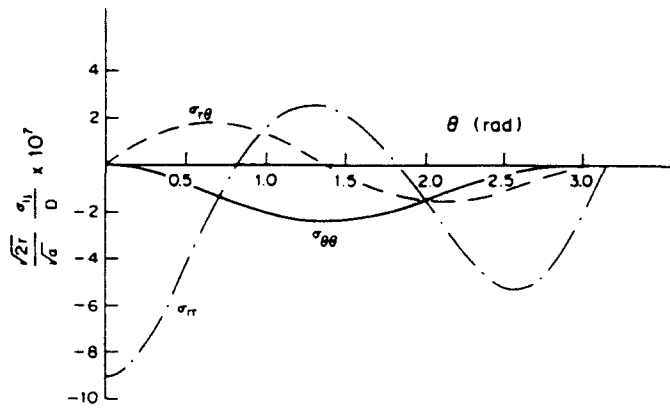Fig. 3. Electric displacement behavior under a tensile load.

Fig. 4. Stress behavior under an electrical load.

3.2. Far-field electrical load

Figures 4 and 5 describe the variations of stress and electric displacement, respectively, when the material is subjected to an electrical displacement $D_2^{(e)} = \mathscr{D} > 0$, that is, in the direction of the (intrinsic) material's polarization vector. In this case $C_i = A_{ij}K_c$. Note that the application of an electric displacement as an external load is equivalent to the application of surface charges on the boundary of the piezoelectric. In practice this is not achievable and, therefore, the external electrical load is produced by means of electrodes attached to the boundary of the ceramic and subjected to a DC voltage that will produce an electric field. For purpose of analysis the manner in which the load is applied is irrelevant. The values of E which correspond to the applied D can be obtained by means of (A1). It can be observed that this kind of external load induces stresses which are usually 10-100 times smaller than those produced by mechanical means, and that the hoop stress $\sigma_{\theta\theta}$ is compressive for all values of θ. A reversal in the sign of $\mathscr{D}$ (obtained by switching the polarity of the electrodes), however, produces a reversal in the sign of the stress components. The maximum magnitude of $\sigma_{\theta\theta}$ occurs at approximately 80° when $\sigma_{r\theta} = 0$. It is important to remark that the magnitude of the applied electrical voltage should produce values of E that remain below 10^6 V m^{-1}, which is the electric field needed to produce the poling of the ceramic. Higher values of E will result in dielectric breakdown.

3.3. Combined mechanical and electrical loads

This example is of fundamental importance in providing an analytical verification of experimentally observed phenomena such as crack arrest and crack skewing (McHenry and
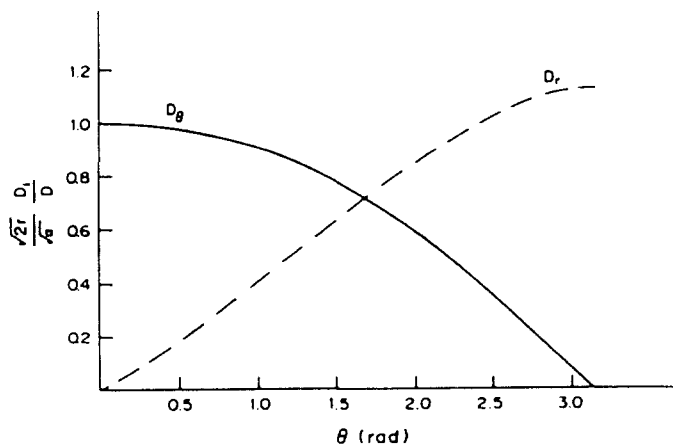

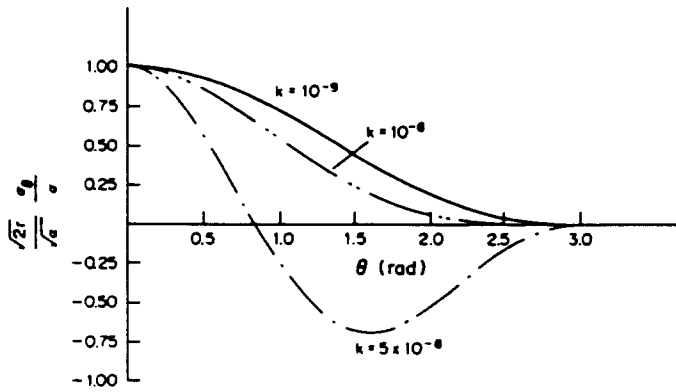Fig. 5. Electric displacement behavior under an electrical load.

Fig. 6. Hoop stress behavior under combined load : $\sigma > 0$, $\mathscr{D} > 0$; $k = \mathscr{D}/\sigma$.

Koepke, 1983). To this end only values of $\sigma_{\theta\theta}$ are important. Figure 6 corresponds to loading conditions $\sigma_{22}^{(\infty)} = \sigma > 0$ and $D_2^{(\infty)} = \mathscr{D} > 0$, that is, $C_j = \Lambda_{j1}K_1 - \Lambda_{j3}K_e$. The normalized value of the hoop stress is plotted for various ratios of $k = \mathscr{D}/\sigma$. Note that for some values of k (in the figure only one such curve is plotted) compressive stresses are observed even though the applied mechanical load σ is tensile. A reversal of the electric load while keeping $\sigma > 0$ will produce only tensile stresses as shown in Fig. 7. Furthermore, it is observed that there exist values of k for which the maximum $\sigma_{\theta\theta}$ is achieved at angles $\theta \neq 0$, suggesting the possibility that the crack will be "turned" towards a direction opposite to that of the applied field.

3.4. Far-field shear load

This particular example appears to be of academic rather than practical interest. Indeed, the simulation of shear load in experimental fracture mechanics poses serious difficulties. First, let the applied load be given by $\sigma_{12}^{(\infty)} = \tau$, thus $C_j = \Lambda_{j2}K_{11}$. In this case it is natural to look for the variation of $\sigma_{r\theta}$ which is depicted in Fig. 8 with the label $\alpha = 0$. If in addition to the shear stress an electric displacement $\mathscr{D}$ is applied, then $C_j = \Lambda_{j2}K_{11} - \Lambda_{j3}K_e$ and it is found that the maximum $\sigma_{r\theta}$ occurs at values of $\theta \neq 0$ as is shown by the other two curves in Fig. 8, where $\alpha = \mathscr{D}/\tau$. Finally, Fig. 9 shows the corresponding behavior of $\sigma_{\theta\theta}$. A comparison of these last two figures shows that under this combined load there are values of θ for which a compressive hoop stress exists with magnitude $|\sigma_{\theta\theta}| > |\sigma_{r\theta}|$. This means that changing the direction of the applied shear load or changing the direction of $\mathscr{D}$ will produce crack skewing and a mode I fracture will prevail over a mode II. Moreover, it is found that this effect is enhanced with an increase in the intensity of $\mathscr{D}$.
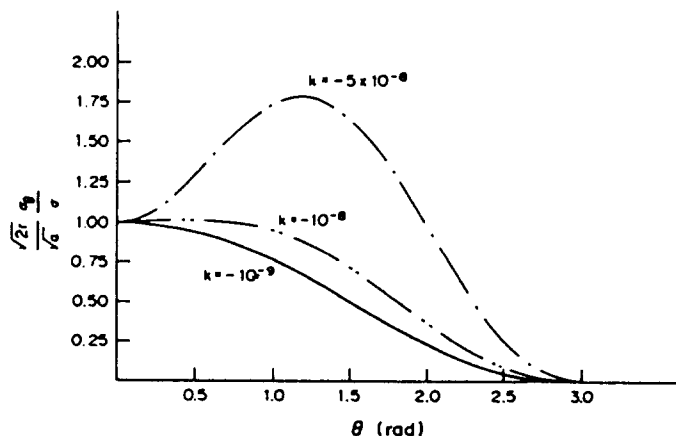

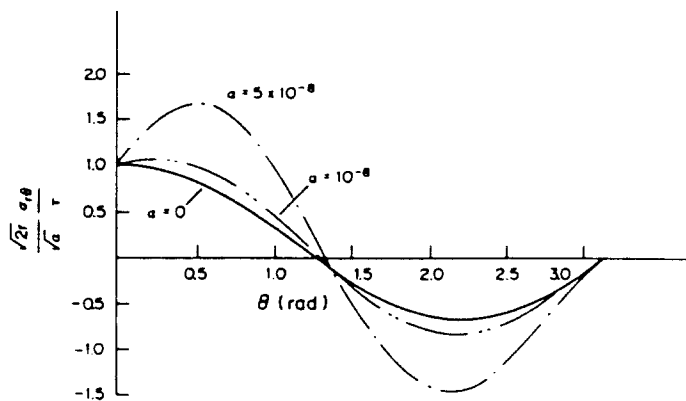Fig. 7. Hoop stress behavior under combined load : $\sigma > 0$, $\mathscr{D} < 0$; $k = \mathscr{D}/\sigma$.

Fig. 8. Shear stress behavior under combined load : $\tau > 0$, $\mathscr{D} > 0$; $\lambda = \mathscr{D}/\tau$.
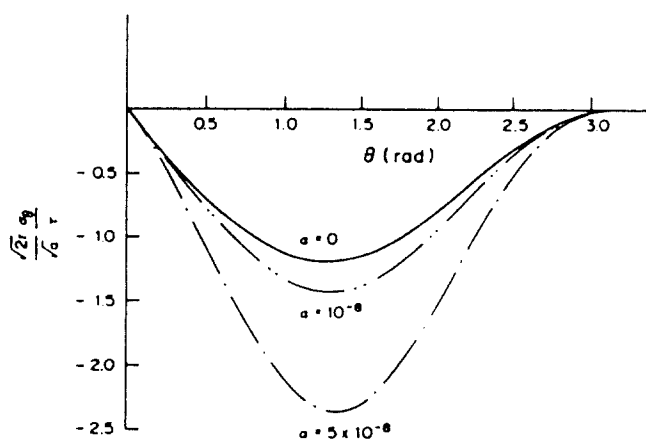

Fig. 9. Hoop stress behavior under combined load : $\tau > 0$, $\mathscr{D} > 0$; $\lambda = \mathscr{D}/\tau$.

4. CONCLUDING REMARKS

Despite the complexity of the piezoelectric phenomena, which embraces material anisotropy as well as coupling effects, the expressions for the crack-tip electromechanical fields are remarkably simple. A high degree of confidence in the results provided in this article stems from three facts: First, eqns (11) as well as those for the elastic displacement reduce to the case of anisotropic fracture mechanics when electrical effects are neglected. Second, during the course of this investigation the author learned that examples (3.1)-(3.3) were also studied by Pak (1992), where the analytical model is based on the method of distributed dislocations. When the same piezoceramic is considered, numerical analysis has shown that both models yield exactly the same results. Third, for the case described in example (3.3) there is experimental evidence that corroborates the present analytical predictions.

REFERENCES

Berlincourt, D. A., Curran, D. R. and Jaffe, H. (1964). Piezoelectric and piezoceramic materials and their function in transducers. In *Physical Acoustics* (Edited by W. P. Mason), Vol. 1-A. Academic Press, New York.
Deeg, W. F. (1980). The analysis of dislocation, crack and inclusion problems in piezoelectric solids. Ph.D. Thesis, Stanford University, CA.
McHenry, K. D. and Koepke, B. G. (1983). Electric fields effects on subcritical crack growth in PZT. In *Fracture Mechanics of Ceramics* (Edited by R. C. Bradt, D. P. Hasselman and F. F. Lange), Vol. 5, pp. 337–352.
McMeeking, R. M. (1989). Electrostrictive stresses near crack-like flaws. *Z. Angew. Math. Phys.* **40**, 615–627.
Pak, Y. E. (1990). Crack extension force in a piezoelectric material. *J. Appl. Mech.* **57**, 647–653.

Pak, Y. E. (1992). Linear electroelastic fracture mechanics of piezoelectric materials. *Int. J. Fract.* **54**, 79–100.

Parton, V. Z. (1975). Fracture mechanics of piezoelectric materials. *Acta Astro.* **3**, 671–683.

Parton, V. Z. and Kudryatvsev, B. A. (1988). *Electromagnetoelasticity.* Gordon and Breach, New York.

Shindo, Y., Ozawa, E. and Nowacki, J. P. (1990). Singular stress and electric fields of a cracked piezoelectric strip. *Appl. Electromag. Mater.* **1**, 77–87.

Sih, G. and Liebowitz, H. (1968). Mathematical theories of brittle fracture. In *Fracture. An Advanced Treatise* (Edited by H. Liebowitz), Vol. II. Academic Press.

Sosa, H. (1991). Plane problems in piezoelectric media with defects. *Int. J. Solids Structures* **28**, 491–505.

Sosa, H. A. and Pak, Y. E. (1990). Three-dimensional eigenfunction analysis of a crack in a piezoelectric material. *Int. J. Solids Structures* **26**, 1–15.

Suo, Z., Kuo, C.-M., Barnett, D. M. and Willis, J. R. (1992). Fracture mechanics for piezoelectric ceramics. *J. Mech. Phys. Solids* (in press).

APPENDIX

The assumption of plane strain conditions reduces (1) to

$$
\begin{Bmatrix} \varepsilon_{11} \\ \varepsilon_{22} \\ 2\varepsilon_{12} \end{Bmatrix} = \begin{pmatrix} a_{11} & a_{12} & 0 \\ a_{12} & a_{22} & 0 \\ 0 & 0 & a_{33} \end{pmatrix} \begin{Bmatrix} \sigma_{11} \\ \sigma_{22} \\ \sigma_{12} \end{Bmatrix} + \begin{pmatrix} 0 & b_{21} \\ 0 & b_{22} \\ b_{13} & 0 \end{pmatrix} \begin{Bmatrix} D_1 \\ D_2 \end{Bmatrix}.
$$

$$
\begin{Bmatrix} E_1 \\ E_2 \end{Bmatrix} = -\begin{pmatrix} 0 & 0 & b_{13} \\ b_{21} & b_{22} & 0 \end{pmatrix} \begin{Bmatrix} \sigma_{11} \\ \sigma_{22} \\ \sigma_{12} \end{Bmatrix} + \begin{pmatrix} \delta_{11} & 0 \\ 0 & \delta_{22} \end{pmatrix} \begin{Bmatrix} D_1 \\ D_2 \end{Bmatrix}.
\tag{A1}
$$

where x_2 is the axis of transverse isotropy or poling axis and the new material constants are given by

$$
a_{11} = s_{11} - \frac{s_{12}^2}{s_{11}}, \quad a_{12} = s_{11} - \frac{s_{12}s_{11}}{s_{11}}, \quad a_{22} = s_{11} - \frac{s_{11}^2}{s_{11}}, \quad a_{33} = s_{44},
$$

$$
b_{21} = \left(1 - \frac{s_{12}}{s_{11}}\right)g_{11}, \quad b_{22} = g_{11} - \frac{s_{11}}{s_{11}}g_{11}, \quad b_{13} = g_{15}, \quad \delta_{11} = \beta_{11}, \quad \delta_{22} = \beta_{11} + \frac{g_{11}^2}{s_{11}}.
\tag{A2}
$$

Consider an elliptical hole in the piezoelectric solid, with semi-axes a and b directed along the x_1 and x_2-axes, respectively. It can be shown (Sosa, 1991) that when loads $\sigma^{(\infty)}$ and $D^{(\infty)}$ are applied to the solid, the electrical and mechanical fields can be expressed in terms of three complex potentials, namely:

$$
\varphi_j(z_j) = (B_j + iB_j^*)z_j + [\Lambda_{j1}l_1 + \Lambda_{j2}l_2 + \Lambda_{j3}l_3]\frac{z_j - \sqrt{z_j^2 - (a^2 + \mu_j^2 b^2)}}{a + i\mu_j b}; \quad j = 1,2,3,
\tag{A3}
$$

where B_j and B_j^* are real constants that are determined from the far-field boundary conditions, Λ_{11}, Λ_{12}, etc., are the elements of the matrix

$$
[\Lambda_{jk}] = \frac{1}{\Delta}\begin{pmatrix} \mu_2\lambda_3 - \mu_3\lambda_2 & \lambda_2 - \lambda_3 & \mu_3 - \mu_2 \\ \mu_3\lambda_1 - \mu_1\lambda_3 & \lambda_3 - \lambda_1 & \mu_1 - \mu_3 \\ \mu_1\lambda_2 - \mu_2\lambda_1 & \lambda_1 - \lambda_2 & \mu_2 - \mu_1 \end{pmatrix},
\tag{A4}
$$

with

$$
\Delta = (\lambda_2 - \lambda_3)\mu_1 + (\lambda_3 - \lambda_1)\mu_2 + (\lambda_1 - \lambda_2)\mu_3,
\tag{A5}
$$

and

$$
\lambda_j = -\frac{(b_{21} + b_{13})\mu_j^2 + b_{22}}{\delta_{11}\mu_j^2 + \delta_{22}}.
\tag{A6}
$$

Furthermore, l_1, l_2 and l_3 are load-geometry related coefficients given by

$$
l_1 = -\frac{a\sigma_{22}^{(\infty)}}{2} + i\frac{b\sigma_{12}^{(\infty)}}{2}, \quad l_2 = \frac{a\sigma_{12}^{(\infty)}}{2} - i\frac{b\sigma_{11}^{(\infty)}}{2}, \quad l_3 = \frac{aD_2^{(\infty)}}{2} - i\frac{bD_1^{(\infty)}}{2}.
\tag{A7}
$$

The components of σ, D and E, as well as of the elastic displacement u and electrostatic potential ϕ are given by (where $\Re$ denotes the "real part"):

$$
\sigma_{11} = 2\Re\sum_{j=1}^{3}\mu_j^2\varphi_j'(z_j), \quad \sigma_{22} = 2\Re\sum_{j=1}^{3}\varphi_j'(z_j), \quad \sigma_{12} = -2\Re\sum_{j=1}^{3}\mu_j\varphi_j'(z_j).
\tag{A8}
$$

$$
D_1 = 2\Re\sum_{j=1}^{3}\lambda_j\mu_j\varphi_j'(z_j), \quad D_2 = -2\Re\sum_{j=1}^{3}\lambda_j\varphi_j'(z_j).
\tag{A9}
$$

$$E_1 = 2\Re \sum_{i=1}^{3} r_i \varphi_i'(z_i), \quad E_2 = -2\Re \sum_{i=1}^{3} s_i \varphi_i'(z_i). \tag{A10}$$

$$u_1 = 2\Re \sum_{i=1}^{3} p_i \varphi_i(z_i), \quad u_2 = 2\Re \sum_{i=1}^{3} q_i \varphi_i(z_i), \quad \phi = -2\Re \sum_{i=1}^{3} r_i \varphi_i(z_i), \tag{A11}$$

where

$$p_i = a_{11}\mu_i^2 + a_{12} - b_{21}\lambda_i, \quad q_i = \frac{a_{12}\mu_i^2 + a_{22} - b_{22}\lambda_i}{\mu_i}.$$

$$r_i = (b_{11} + \delta_{11}\lambda_i)\mu_i, \quad s_i = b_{21}\mu_i^2 + b_{22} + \delta_{22}\lambda_i. \tag{A12}$$